Asian Journal of Pharmaceutical Sciences 17 (2022) 139–152

Available online at www.sciencedirect.com

ScienceDirect

journal homepage: www.elsevier.com/locate/AJPS

Original Research Paper

The enhancing effect and promoting mechanisms of the stereoisomeric monoterpene alcohol esters as enhancers for drugs with different physicochemical properties

Heping Wang[a,1], *Yan Li*[b,1], *Chunyan Wang*[b], *Jing Wang*[a], *Bo Ren*[a], *Xiaona Li*[a], *Mingzhu Li*[b], *Dandan Geng*[a], *Chensi Wu*[a], *Ligang Zhao*[a,c,*]

[a] *School of Pharmacy, North China University of Science and Technology, Tangshan 063000, China*
[b] *Dept of Pharmacy, Tangshan Maternal and Child Health Hospital, Tangshan 063000, China*
[c] *Tangshan key laboratory of novel preparations and drug release technology, Tangshan 063000, China*

ARTICLE INFO

Article history:
Received 2 August 2021
Revised 15 October 2021
Accepted 5 November 2021
Available online 9 December 2021

Keywords:
O-acylgeraniol derivatives
O-acylnerol derivatives
Transdermal drug delivery system
In vitro and *in vivo* correlation
Enhancing mechanism

ABSTRACT

To explore the structure-activity connections of amphiphilic permeation enhancers containing the length of the hydrophobic chains as well as the properties of the polar head, *O*-acylgeraniol and *O*-acylnerol derivatives were synthesized from geraniol/nerol (*cis*-isomer of geraniol) and pharmaceutical excipient acids in this research. Their promotion of the percutaneous absorption of three drugs as the model, flurbiprofen (FP), isosorbide dinitrate (ISDN) and donepezil (DNP), which were selected based on their physicochemical properties, was tested by *in vitro* skin penetration and *in vivo*. Molecular simulation, ATR-FTIR, CLSM and histological observation were implement to evaluate the mode of action of the enhancers. The results indicated that *(E)-3,7-dimethyl-2,6-octadien-1-yl tetradecanoate* (GER-C14, *trans*-) achieved the highest enhancement ability for the three drugs; additionally, the *in vivo* results obtained were in good correlation with the *in vitro* data. Molecular docking results suggested that enhancers loosen the hydrogen bonds between ceramides, and the results of molecular simulation indicated that GER-C14, NER-C14 could insert into the middle of the lipid bilayer to form an independent phase. According to ATR-FTIR and histological evaluation, the enhancers extracted lipids and influenced the protein region, thereby disturbing the skin array. In addition, CLSM described the dynamic effects of enhancers on lipids between stratum corneum (SC) cells. In conclusion, GER-C14 had a better penetration promotion effect, which broadened our understanding of stereoisomeric penetration enhancers.

* Corresponding author.
E-mail address: tsyxzlg@163.com (L.G. Zhao).
[1] These authors contributed equally to this work.
Peer review under responsibility of Shenyang Pharmaceutical University.

https://doi.org/10.1016/j.ajps.2021.11.003

1. Introduction

Transdermal drug delivery systems (TDDSs) are indispensable in current controlled drug delivery systems [1–3]. This noninvasive drug delivery system offers many superior properies, for example, good patient obedience, stable blood concentration and prevention of first-pass effects [4]. However, the SC is the foremost obstacle in the surface of skin for drug permeation [5]. Several tactics were exploited to address the awesome obstacle features by the SC. A kind of way is to add chemical penetration enhancers to the prescription, which could increase the permeability of the drug through various levels, involving breakage of the lipid bilayer, fluidization, lipid abstraction, etc. [6]. Terpene compounds, which are existing in benzine, as penetration enhancers because of their safety and effectiveness [7]. The effect of certain terpene compounds on skin was decided to their functional group, and physicochemical properties have been reported [8].

As one of the terpenes, geraniol (GER) or nerol (NER, a *trans*-isomer of GER) has been studied as an enhancer for drugs such as diclofenac sodium [9], caffeine and triamcinolone acetonide [10]. However, few studies have systematically discussed the relationship between the structure-activity (the influence of double bond geometry) of penetration enhancers. In this study, GER/NER and fatty acids were chosen as lead compounds to synthesize new kinds of *O*-acylgeraniol and *O*-acylnerol derivatives as candidates for permeation enhancement. The long alkyl chain part and the polar part with configurations isomerism were considered essential for its actions as a penetration enhancer [5]. To study the effectiveness of it, the enhancement of the skin penetration of three drugs with different physicochemical properties was examined in this report. The three model drugs were flurbiprofen (FP) [11], donepezil (DNP) [12], and isosorbide dinitrate (ISDN) [13], which had previously been proven in percutaneous absorption, and the physicochemical parameters are presented in Table 1.

In this study, an *in vitro* skin penetration test using rabbit skin was used to optimize the formulation of the patch. Then, the pharmacokinetic behavior of optimized FP patches was determined using an animal model. More importantly, *in vitro* drug release experiments, ATR-FTIR, MS and CLSM were conducted to characterize the interaction among the selected enhancers (GER, NER, GER-C14, NER-C14) and SC. The goal of the research was to exploit a penetration enhancer for different physicochemical drugs and to reveal the mechanism of permeability promotion. This systematic experiment was the first research on the infiltration ability and mechanism of configurational isomerization enhancers on drugs with different physicochemical properties, which had great significance in the clinical application of configurational isomerization enhancers.

Table 1 – Physicochemical properties of FP, DNP and ISDN.

Parameters	Drugs FP	DNP	ISDN
Melting point (°C)	110	223–227	70
MW (g/mol)	244.26	379.49	236.14
LogP at 32 °C	4.16	3.91	1.34
pK_a [a]	4.42	8.84	–

[a] Calculated using ACD/Lab software

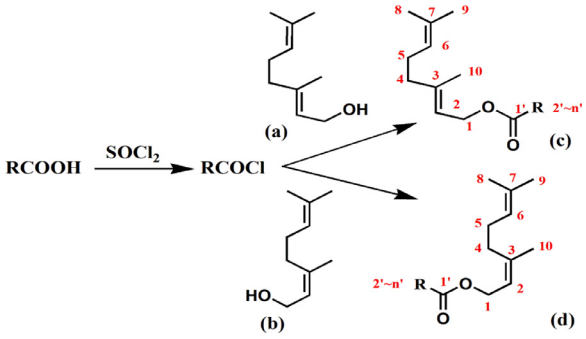

Fig. 1 – The synthesis of GER/NER ester derivatives. (a) GER; (b) NER; (c) *O*-acylgerniol derivatives; (d) *O*-acylnerol derivatives.

2. Materials and methods

2.1. *Materials*

DURO-TAK 87-235A, 87-2052, 87-4287, was purchased from Henkel Co., Ltd (New Jersey, USA); Isopropyl paraben was obtained from Tianjin Aobin pharmaceutical distribution Co., Ltd. (Tianjin, China); Butyl p-hydroxybenzoate, FP, ISDN, DNP•HCL, GER, NER were obtained from Beijing merida technology Co., Ltd. (Beijing, China); C6-C14 fatty acids, oleic acid and thionyl sulfoxide were purchased from Airan Biotech reagent Co., Ltd (Beijing, China); Methanol (MeOH, chromatographic grade) was obtained from the fisher Co, Ltd (New Jersey, USA); Other reagents meet the standard grade.

2.2. *Preparation of O-acylgeraniol derivatives and O-acylnerol derivatives*

The synthesis reaction was carried out with GER (*trans*)/NER (*cis*) and long-chain fatty acids as the leader compounds to prepare the target products. Because the direct synthesis of GER/NER ester derivatives was difficult, acyl chloride compounds were first synthesized as intermediates. As shown in Fig. 1, the specific reaction process was as follows: fatty acids and thionyl chloride were reacted in an oil bath at 60 °C (3 h). To prevent excess thionyl chloride from remaining in the reaction system, acyl chloride was obtained by vacuum distillation at 45 °C until no droplet remained in the collection bottle. After cooling to 15 °C, acyl chloride was gradually added into GER/NER mixed with triethylamine, and the suitable tetrahydrofuran as the solvent. The reaction system continued to react for 4 h at 75 °C, and the progress of the reaction was verified to be completed

by thin layer chromatography (TLC). To ensure the project was accomplished, the product was dissolved with ethyl acetate (EA), and the pH was adjusted using 5% NaOH solution (w/v) to 8.0. The upper was collected and washed twice, and the EA was except after drying for 6 h with magnesium sulfate. The target products were separated by column chromatography. The constructions of *O*-acylgeraniol derivatives and *O*-acylnerol derivatives were verified by NMR (JNM-ECZR, Jeol, Japan). The spectrogram construction was detailed in Supplementary Material.

2.3. *In vitro skin permeation experiments*

2.3.1. *Preparation of skin*

The Experimental Animal Center of North China University of Science and Technology provided Japanese white rabbits (male, 2.5–3.0 kg), and all experiments were in light of the 'Ethical Guide for Laboratory Animal Investigation'.

The skin was obtained from the back. To guarantee the completeness of skin, the back hair was carefully removed using a pet trimmer and razor when the rabbit was in anesthesia (by inhaling diethyl ether). After the rabbit was deceased and the subcutaneous fat was weeded out, the full thickness of the skin was removed. The obtained skin was frozen at −80 °C for later use. Prior to the skin permeation research, the frozen skin was in physiological saline to thaw for 20 min.

2.3.2. *Preparation of drug-in-adhesive patches*

The effects of enhancers on FP, DNP and ISDN percutaneous absorption were investigated using acrylic adhesives (DURO-TAK 87–235A, 87–4287, 87–2052, PSA), which were screened by pre-experiment. In addition, the drug loading was set to 150, 150 and 50 mg after the pre-experiment ($n = 4$), and the concentrations of GER/NER were set at 3%, 3% and 1% (w/w). The drug and enhancer were added in EA and then mixed with PSA. Then, each component was stirred for 15 min until it became well proportioned. The air bubble in the mixture was removed by letting it sit for 10 min and pouring on the silicone-coated liner. Then, the film was placed in an oven to dry at 50 °C (15 min). After that, a backing film (Scotch Pak®9733,3 M) was covered on the PSA layer. Patch thickness measurement: The thickness of FP, DNP, and ISDN patches were measured four times at different places. Calculated the average value, and then subtracted the thickness of the backing layer and the anti-adhesive layer. During the experiment, the thickness of all patches were 100 ± 10 μm.

Crystal observation: The patches were stored at room temperature, and observed once a week. An optical microscope (Shanghai Optical Instrument Sixth Factory) was used to observe under the magnification of the eyepiece objective lens. There was no crystallization in all the patch during the stored period.

2.3.3. *In vitro permeation experiment*

Horizontal dual-chamber diffusion cells with an actual diffusion area of 0.95 cm^2 were used, and rabbit skin was installed on the receiving cell with the SC facing outward. The tested patch was put up on the surface of the skin prudently to prevent bubbles from appearing between them. After clamping the cells together securely, 3.5 mL of phosphate buffer solution (PBS, pH=7.4) was added to the receiving cell and stirred with a magnetic rotor. Sample collection times were 2, 4, 6, 8, 10, 12 and 24 h. A 2.0 ml sample was taken, and the PBS (2.0 ml) was replenished.

2.3.4. *Data analysis*

The permeability curve was plotted as the cumulative transmittance per unit area (Q), as shown in Eq. 1:

$$Q_{24h} = (3.5C_i + 2.0\sum_{i=1}^{n-1} C_{i-1})/A \quad (1)$$

where C_i and C_{i-1} are the concentrations of samples at i h and i-1 h, V_i is the single sampling volume (2.0 ml), V is the capacity of the diffusion pool (3.5 ml), and A is the diffusion area (0.95 cm^2).

The enhancement ratio (*ER*) was to appraise the ability of the enhancer as shown in Eq. 2

$$ER = Q_{24h}(\text{with enhancer})/Q_{24h}(\text{without enhancer}) \quad (2)$$

The steady-state flux (*Js*, μg/cm^2/h) was depending on the line segment with the highest coefficient. The lag time (T_{lag}) was the linear part extrapolated to the point where it intersected the *X*-axis.

Results were showed as the mean ± standard deviation. The *t*-test was employed for statistical analysis of the data with SPSS 17.0 software. The level of significance was defined as $P < 0.05$.

2.4. *In vivo studies*

2.4.1. *Instructions of patches*

Thirty Japanese white rabbits (male, 2.5 ± 0.2 kg) were partitioned into 5 groups, and patches were applied with or without enhancer: (1) control group: only FP was used; (2) the patch was prepared with GER; (3) the patch was prepared with NER; (4) the patch was prepared with GER-C14; and (5) the patch was prepared with NER-C14. Patches of 80 cm^2 (including 208.8 mg FP) were placed on the shaved abdominal skin of rabbits.

The blood sample (1.5 ml) was obtained from the auricular vein of rabbits at 0.5, 1, 2, 4, 6, 8, 12, 16, 20, 24, 26, 28, 30, 32, 36 and 48 h, and the patch was ripped off at 24 h after administration. After centrifugation for 5 min (4 °C, 14 000 rpm), 200 μl of plasma sample was obtained and then stored at −80 °C.

2.4.2. *Plasma sample extraction*

20 μl of internal standard solution (butyl p-hydroxybenzoate, 20 μg/ml), 400 μl of chromatographic grade methanol and 100 μl of plasma were vortex for 5 min. After centrifugation at 14 000 rpm for 15 min, the upper was evaporated to dryness under nitrogen at 40 °C, then redissolved in chromatographic grade methanol (100 μl), vortexed for 5 min, and centrifuged for 15 min (4 °C, 14 000 rpm). Finally, the clarified solution sample (20 μl) was analysis by HPLC.

2.4.3. *Pharmacokinetic analysis*

Pharmacokinetic parameters containing the biggest plasma drug concentration (C_{max}) and the time to C_{max} (T_{max}) were calculated directly from the plasma concentration-time profile. According to the noncompartmental model, WinNonlin®7.0 software (Pharsight Corporation, San Diego, CA, USA) was to calculate other pharmacokinetic parameters, including the mean residence time (*MRT*), which measures drug absorption extent, plasma clearance rate (*Cl*), apparent volume of distribution (*V*) and the area under the time-concentration curve from time 0 to time t ($AUC_{0\text{-}t}$). In addition, the enhancement factor (E_f) was calculated by Eq. 3, and the absolute bioavailability (*F*%) was calculated by Eq. 4:

$$E_f = AUC_{0-t}(\text{with enhancer})/AUC_{0-t}(\text{without enhancer}) \quad (3)$$

$$F\% = (AUC_{patch} \times D_{iv})/(AUC_{iv} \times D_{patch}) \times 100 \quad (4)$$

AUC_{patch} and AUC_{iv} represent the $AUC_{0\text{-}t}$ under patch administration and intravenous injection, respectively, and *D* represents the dosage.

2.4.4. *IVIVC*

In vitro and *in vivo* correlation (IVIVC) was constructed using a noncompartmental model, and deconvolution was used [14]. According to the algorithm, *in vitro* permeability (*vitro*%) and *in vivo* permeability (*vivo*%) were obtained. *Vitro*% was an independent variable, *vivo*% was a dependent variable, and the correlation coefficient was calculated *in vitro* and *in vivo*.

2.5. *Drug release*

The FP, ISDN and DNP patches with or without penetration enhancers (GER, NER, GER-C14 and NER-C14) were selected for *in vitro* release measurement. The experimental device was a dissolution tester (Ai Laibao, Jinan, China). The patch was immersed in PBS (pH=7.4, 900 ml) into a dissolution cup and preheated to 32±0.5 °C. Samples of 5 mL were collected at 0.5, 1, 2, 4, 6, 8, 10, 12 and 24 h and then replaced with fresh PBS of the same volume. Samples were centrifuged at 4000 rpm for 5 min. Then, 300 µl upper and 300 µl internal standard solution was mixed. Liquid phase analysis was conducted.

2.6. *HPLC analysis*

2.6.1. *In vitro*

High-pressure liquid chromatography (HPLC) was used to quantify the model drugs. The HPLC system included a Shimadzu liquid chromatograph and Shimadzu software. The HPLC was provided with a UV detector (SPD-20A), a pump (LC-20AT), an automatic injector (SIL20A), and a column oven (CTO-20A). A reversed-phase C_{18} column (5 µm, 4.6 mm × 150 mm, Thermo Fisher, USA) was used. The drug content was determined by the internal standard method. The specific chromatographic conditions for the three model drugs are shown in Table 2 when experiments were carried out *in vitro*.

Table 2 – Chromatographic conditions of model drugs.

Drug	Mobile phase (*v/v*)	Temperature (°C)	Wave length (nm)	Internal standard	Flow rate (ml/min)
FP	MeOH:1%HAC (55:45)	40	247	Prophy paraben	1
DNP	MeOH:10 mM NH_4OAc (92:8)	40	271	Prophy paraben	1
ISDN	MeOH:H_2O (25:75)	40	230	Prophy paraben	1

2.6.2. *In vivo*

In *in vivo* drug absorption experiments, the instruments and chromatographic columns used for the determination of FP content were the same with the *in vitro*. The mobile phase was MeOH:1% HAC (23:73, v/v), and the flow rate was 1 ml/min. The wavelength was set to 254 nm. The retention time for FP was 22 min.

2.7. *Identification of drug-SC interaction*

2.7.1. *Molecular docking*

Molecular docking was to test the interplay of drug, lipids and the stability of the skin lipid bilayer after adding the penetration enhancer by using Materials Studio version 7.0 software. The structures of ceramide NPs (CER NPs), model drugs and enhancers were built by means of ChemDraw 16.0, majorization by the Forcite module, and molecular docking was occurred in the Blend functional area to find the optimal combination location. The lowest energy conformation of the mixture in which the frequency of blends was adjusted to 1000 and all other parameters were set to the default settings under the COMPASS II force field was determined. Finally, the docking energy was calculated under the Dreiding force field.

2.7.2. *Molecular dynamics simulation*

Molecular dynamics simulation was used to explore the interaction between enhancers and skin protein. The initial coordinates of the equilibrated 128DPPC bilayer were received from Tieleman's group (http://wcm.ucalgary.ca/tieleman/downloads). Materials Studio version 7.0 software was used to construct the structure of the enhancer and optimize it with the Forceite II force field. The structure of 128DPPC and penetration enhancer was mixed in autodock tools 1.5.6.

2.8. *ATR-FTIR*

The rabbit back hair was removed and partitioned into 5 regions with a size of 1.0 cm^2 each. Permeation enhancers (GER, NER, GER-C14, NER-C14) were dissolved in ethanol (3%, w/w), and pure ethanol-treated skin was used as a control. Twenty microliters of the solution was added onto the symbol area for an unveiled time of 30 min. Then, the skin was wiped with tissue paper. The samples were placed onto ZnSe crystals at an incident angle of 45° The spectra were collected over

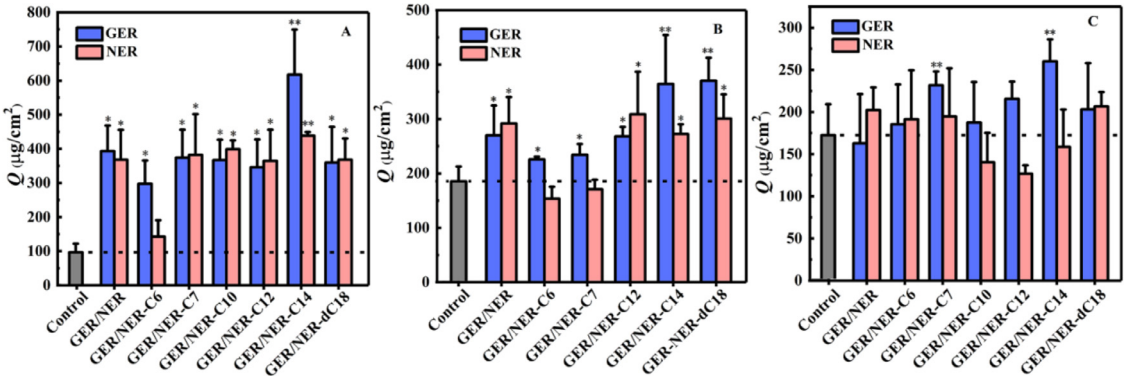

Fig. 2 – Q_{24h} of drugs in patches with or without enhancers through skin. (A) FP; (B) DNP; (C) ISDN (mean±SD, $n = 4$).* represents a significant difference from the control group; ** represents a significant difference from the group containing GER or NER, $P<0.05$.

the wavenumber region of 4000–1000 cm^{-1} by averaging 200 scans by a Thermo Nicolet NEXUS 470 spectrometer (Madison, USA).

2.9. CLSM

The saturated fluorescein solution was prepared with isopropyl palmitate (IPP) as the solvent. The skin prepared in the "2.3.1" section was mounted in vertical diffusion cells. Then, 600 μl supernatant fluorescein solution was smeared to the skin. After 10 min, the solution was discarded, and then the skin was rinsed with distilled water and dried with filter paper. Place the skin sample on the glass slide. Skin imaging was presented on an Olympus FV1000 Laster Scan Microscope (Thermo Nexus+70, America). The excitation wavelength was set at 488 nm. Z stacks of the samples were taken from the SC to the dermis.

2.10. Histological study

To determine the irritation of enhancers on skin, histological research was conducted. The rabbit back hair was removed and divided into 5 areas with a size of 1.0 cm^2 each. Anhydrous ethanol solution (20 μl) with or without enhancers (GER, NER, GER-C14, NER-C14) was applied to the skin for 1 h, and then the residual enhancer was cleaned up with absorbent cotton. The application site was excised and fixed in paraformaldehyde solution (4%). One day after fixation, the application sites were embedded in paraffin at a vacuum of 60 °C for 30 min. After paraffin vertical coronal sections, they were stained with H&E.

2.11. Skin irritation test

Five Japanese white rabbits (half male and half female) were partitioned into 5 groups, divided into four areas on either side of the spine, and applied 250 μl ethanol solution that with or without enhancer (The mass fraction of enhancer was 3%). The administration site was fixed with medical gauze and tape. The enhancer was wiped off with cotton ball at 24 h after administration, and then the skin of tesr area was observed at 2 h, 12 h, 24 h and 48 h.

3. Results and discussion

3.1. In vitro permeation study

The influence of enhancers on the penetration of the three model drugs is shown in Fig. 2, and the penetration parameters (*Js*, T_{lag}, *ER*) are listed in Table 3. The parent enhancer GER/NER enhanced the FP and DNP significantly over the control; the *ER* values of GER to FP, DNP were 4.06 and 3.80, the ER of NER to FP, DNP were 1.45 and 1.57, respectively. As shown in Fig. 2A, the skin permeation showed that the FP patches with the enhancer (except NER-C6) could clearly increase skin penetration over the control ($P<0.05$). The highest cumulative amount was obtained from GER-C14 (*trans*-, 617.78±131.71 μg/cm^2), followed by NER-C14 (*cis*-, 438.55±11.03 μg/cm^2). However, with the exception of C6- and C14- derivatives, GER/NER or other ester derivatives showed no difference in activity to promote permeability. Fig. 2B represented the permeation amount of DNP from patches containing different enhancers. The experimental group containing GER and *O*-acylgeraniol derivatives all promoted the transdermal absorption of DNP ($P<0.05$). Among the experimental group, the Q_{24h} of GER-C14 and GER-*d*C18 on DNP reached 364.60 ± 89.88 μg/cm^2 and 370.37 ± 42.44 μg/cm^2, which were 1.96 times and 2.00 times those of the control, respectively. In addition, GER-C14 and GER-*d*C18 with a *trans* conformation were stronger than the corresponding *cis* structures (NER-C14 or NER-*d*C18) in enhancement effect. Interestingly, when NER-C6 and NER-C7 were used as penetration enhancers, they had no effect on DNP transdermal absorption instead of promoting it. For ISDNs shown in Fig. 2C, GER-C7 and GER-C14 with *trans* conformations had a significant influence on the flux of ISDNs relative to the control. Based on data from skin permeation, for the above three drugs, most of the enhancers had obvious activity in promoting permeability, and the parent enhancer GER/NER did not have significant effects on permeation ($P > 0.05$). Among these drugs, GER-C14 (*trans*-) had the best penetration promoting ability on FP, DNP and ISDN. In addition, GER-*d*C18, GER-C14, GER-C6, and GER-C7 with trans structures sometimes had better

Table 3 – Skin permeate on parameters of the drugs from the patches (Mean±SD, $n=4$).

Enhancers	FP			ISDN			DNP		
	J_s (μg/cm^2/h)	T_{lag} (h)	ER	J_s (μg/cm^2/h)	T_{lag} (h)	ER	J_s (μg/cm^2/h)	T_{lag} (h)	ER
Control	4.72±0.18	3.50	1.00	7.75±1.54	1.79	1.00	9.24±2.54	4.17	1
GER	19.02±2.51*	3.39	4.06	6.90±1.52	0.42	0.94	13.30±2.05*	4.94	1.45
NER	18.89±1.12*	4.72	3.80	8.66±0.81	0.62	1.17	15.75±2.09*	5.98	1.57
GER-C6	15.09±0.84*	4.50	3.07	8.13±1.91	1.27	1.07	1.02±0.06*	0.00	1.21
NER-C6	7.40±1.49	4.94	1.48	8.99±2.69	3.10	1.11	7.14±1.20	2.08	0.82
GER-C7	19.07±1.23*	4.70	3.86	10.99±0.66**	3.32	1.34	11.60±3.07*	3.88	1.26
NER-C7	19.99±2.23*	5.31	3.95	8.16±1.88	0.13	1.12	8.84±2.11	5.10	0.92
GER-C10	19.23±2.56*	5.39	3.79	8.34±2.30	1.61	1.08	–	–	–
NER-C10	19.94±1.39*	4.42	4.12	6.03±1.09	0.70	0.81	–	–	–
GER-C12	17.47±2.57*	4.65	3.57	10.11±0.87	3.06	1.25	14.07±2.14*	5.32	1.45
NER-C12	19.36±3.03*	5.70	3.77	5.47±0.37	0.83	0.73	16.03±2.33*	5.09	1.66
GER-C14	29.64±5.24**	3.44	6.38	12.14±0.90**	2.97	1.50	18.82±3.57**	4.83	1.96
NER-C14	22.59±6.01**	5.03	4.53	6.60±1.70	0.00	0.91	12.22±2.14*	1.54	1.47
GER-*d*C18	18.82±2.51*	5.29	3.71	8.62±1.48	0.63	1.17	19.06±1.53**	4.43	2.00
NER-*d*C18	18.03±2.88*	3.99	3.80	8.56±1.19	0.63	1.19	15.77±1.66*	4.19	1.62

Note: *represents a significant difference from the control group.
** represents a significant difference from the group contain GER or NER, $P<0.05$; - represents not implemented.

penetration promotion capacity than the corresponding *O*-acylnerol derivatives.

Research has shown that the effect of penetration enhancers is not directly proportional to the concentration [15]. When the penetration enhancer effect was stable, the higher the concentration was, the lower the activity of the penetration enhancer, and it could also induce high irritation. Therefore, in the preliminary experiment (not shown), the GER/NER patches were prepared separately with different loads. We determined that the best penetration-enhancing concentrations of GER/NER for the three drugs (FP, DNP, ISDN) were 3%, 3% and 1%. To ensure the comparability of the ester derivatives and the parent compound, in the subsequent experiments, the molar concentration of the ester derivatives was equal to the optimal molar concentration of GER/NER.

It is generally believed that the penetration enhancer has two action sites in the SC: the polar head region and the hydrophobic side chain of the bilayer [16]. Small-molecule polar substances could break the hydrogen bond between ceramides, while amphiphilic penetration enhancers were inserted into the lipid bilayer, and their polar head and hydrophobic tail entered the polar region and hydrophobic region of the lipid bilayer, respectively, which broke the orderly arrangement of lipids, increased the fluidity of the lipid bilayer, and reduced skin barrier function [17]. In addition, enhancers with a high n-octanol/water partition coefficient (log*P*) are distributed well into the SC intercellular lipid domain [18]. The results showed that the penetration-promoting effects of GER and NER were the same, which might be caused by the similar physical and chemical properties of GER and NER. Warner hypothesized that the polar head of the enhancer was the reason for permeation and locating the molecule into the SC lipids and that it does not affect the mechanism of action [19, 20]. The transformation of GER/NER into ester derivatives could improve its lipophilicity, and theoretically, could further improve the penetration-promoting ability. The increasing volume increased the hydrophobic surface, which would enhance partitioning into SC, thus increasing the permeability of the lipid membrane. In contrast, larger molecules required more space and diffused more slowly. The results of *in vitro* permeation showed that GER-C14 had the best penetration promotion effect on the three model drugs. The balance between the size and lipophilicity of the enhancer could provide greater penetration activity. In addition, GER and NER had the same booster effect, and GER-C14 was always better than NER-C14 in penetration-promoting activity, which might be due to the different permeabilities of those enhancers (with the same chain lengths) into their site of action. This effect will be explained in ATR-FTIR, CLSM later.

The model drugs were selected according to the different physicochemical properties, such as, the pKa, solubility, melting point, Log*P*, etc., which were shown in Table 1. The choice of PSA was based on the physicochemical properties of model drugs. PSA were divided into three categories according to the type of functional group: carboxylic acid (DURO-TAK 87-235A, 87-2052) and hydroxyl group (DURO-TAK 87-4287). Drug-PSA interaction was one of the most important factors affecting the skin penetration of drugs. The ionic interaction between basic drugs and carboxyl-containing PSA could inhibit the release of drugs in both kinetics and thermodynamics. Therefore, DNP had almost no skin penetration in DURO-TAK 87-235A and DURO-TAK 87-2052 containing carboxyl groups, and FP had almost no skin penetration in DURO-TAK 87-4287 pressure-sensitive adhesive. In summary, due to the different PSA selected in the patch prepared in the experimental group, it was impossible to compare the difference between the effect of the drug and the enhancer.

Table 4 – Pharmacokinetic parameters of FP patches (mean±SE, $n = 6$).

parameters	Control	NER	GER	NER-C14	GER-C14
T_{max} (h)	9.67±2.44	21.33±3.71	12.67±3.04	12.33±3.44	6.67±2.67
C_{max} (μg/ml)	1.16±0.37	2.62±0.41	5.13±0.85	4.66±0.64	17.50±0.84
AUC_{0-48} (h•μg/ml)	14.62±5.02	45.35±12.74	102.88±27.42	88.16±10.41	283.58±28.65
V (l)	280.30±79.95	58.47±14.26	29.42±6.51	44.52±8.52	16.33±5.14
Cl (l/h)	28.12±10.17	8.55±1.90	4.67±1.73	3.26±0.53	0.97±0.08
MRT (h)	12.99±0.30	18.26±1.89	17.91±1.99	17.85±1.37	17.31±1.18
F%	1.83±0.53	3.69±0.60	12.90±1.44	11.05±1.30	35.55±0.04
E_f	1.00	3.10	7.04	6.03	19.40

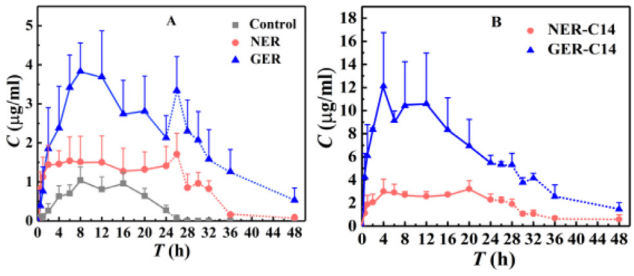

Fig. 3 – Plasma concentration-time profiles in rabbits after transdermal application of FP patches with or without enhancer. The dashed line is the plasma concentration at 24 h after patch removal.

3.2. *Effect on pharmacokinetics*

3.2.1. *Effect on pharmacokinetics*

The patches with or without penetration enhancers were evaluated by pharmacokinetics. The plasma concentration-time curves of FP are indicated in Fig. 3. FP patches with or without penetration enhancers demonstrated totally different drug-plasma concentration profiles. Compared to the control, the patches with penetration enhancers significantly improved C_{max}, especially GER-C14 (17.50±0.84 μg/ml). Pharmacokinetic parameters were listed in Table 4. The main evaluation criterion for skin absorption of drugs *in vivo* was the AUC_{0-t}. The AUC_{0-48} of the control group (14.62±5.02 h•μg/ml) was significantly lower than the AUC_{0-t} of the other groups, especially the GER-C14 group (283.58±28.65 h•μg/ml). In the case of NER and NER-C14, a plateau phase (from 4 h to 20 h) was shown after reaching C_{max} and then declined gradually, which directed the drug to permeate into the skin continuously. However, in the GER and GER-C14 groups, there was no plateau but a rapid decline after reaching C_{max}. The *in vivo* data suggested that GER-C14 had a stronger penetration ability than NER-C14 or others, which was unanimous with the results of *in vitro* permeation, and the bioavailability was the highest. Furthermore, there was no difference in the *MRT* values of different penetration enhancers because the *MRT* values of transdermal patches were related mainly to the time of patch administration and the quality of the drug itself but not to the excipients used [21]. In addition, the plasma concentration still increased after the patch was removed, which indicated that the drug continued to penetrate the skin because of the barrier function of SC, which led to an early accumulation of the drug. In general, the bioavailability of transdermal patches should be more than 40%. However, most of the patches developed in research had low bioavailability, which might be due to: (1) the dosage in the patch is too large to penetrate completely through the skin; or (2) when the patch was removed, there was still a large amount of drug in the patch.

3.2.2. *IVIVC*

Although the final target of enhancing percutaneous absorption is contact with humans, *in vivo* studies are not always feasible for some factors. IVIVC acts as a predictive model representing the connection between the *in vitro* behavior and relational *in vivo* expression [22, 23]. The correlation was obtained, and the results are shown in Fig. 4. The consequents of the IVIVC showed that the *in vitro* permeation test could be used to forecast the *in vivo* performance of patches (R^2>0.8783) [24].

3.3. *In vitro drug release experiment*

Generally, the drug delivery of the patch is facilitated in two ways: enhancing the release of the drug from the patch and enhancing the skin permeability of the drug [25]. Drug release research explained the effect of enhancers (GER, NER, GER-C14, NER-C14) on the FP, DNP, and ISDN release processes. As shown in Fig. 5A & 5C, the release process of FP and ISDN from patches was obviously facilitated by GER-C14 and NER-C14 compared with the other groups, and there was no difference. Notably, the effect of GER-C14 was better than the effect of NER-C14 on FP and ISDN transdermal permeation amounts. These findings indicated that the transdermal process might be the main reason affecting the promotion of drug delivery in patches containing GER-C14 or NER-C14. In Fig. 5B, the release process of DNP was facilitated significantly by GER-C14, followed by NER-C14, which was identical to the effect of DNP transdermal permeation amount. It was possible that both the release and transdermal processes led to this consequence. These results suggested that enhancers may facilitate drug transdermal permeation by promoting the release of the drug from the patch. There were possible reasons for the addition of penetration enhancers to promote the release of the drug from the patches: (1) The addition of penetration enhancer reduced the interplay between the drug and PSA [26]; (2) The penetration enhancer was likely to promote the molecular mobility of PSA, which introduced a higher frequency of free volume formation in the PSA [27]. These hypotheses need

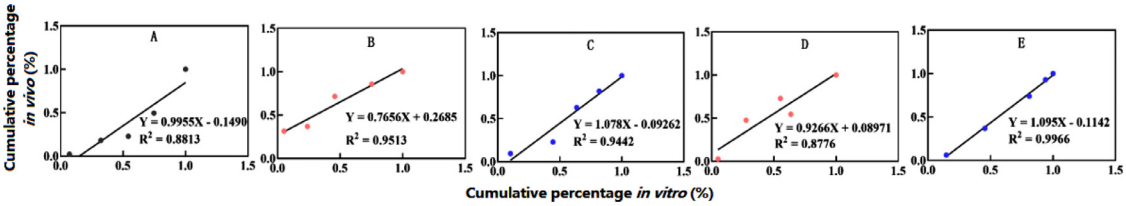

Fig. 4 – IVIVC analysis of FP patches with or without enhancer. (A) control; (B) NER; (C) GER; (D) NER-C14; (E) GER-C14.

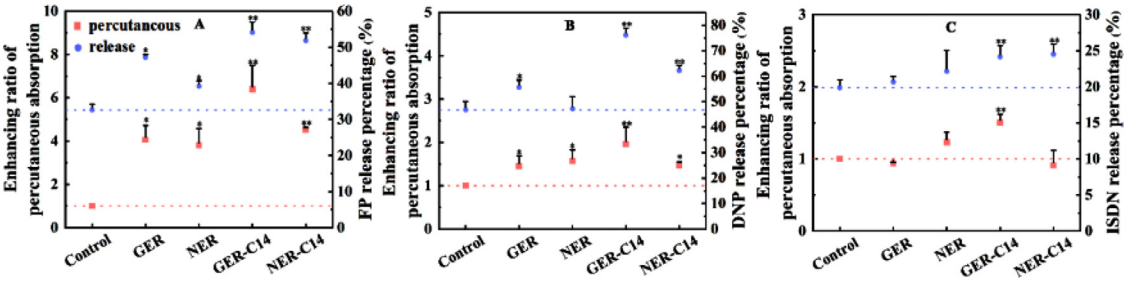

Fig. 5 – The relationship of drug release and drug skin permeation.(A) FP; (B) DNP; (C) ISDN; * represents a significant difference from the control group; ** represents a significant difference from the group containing GER or NER, $P<0.05$.

Table 5 – The hydrogen-bond energy.

Group	Hydrogen-bond energy	Group	Hydrogen-bond energy	Group	Hydrogen-bond energy
FP-NP	−1.208	DNP-NP	−1.176	ISDN-NP	−1.159
FP-GER-NP	−1.519	DNP -GER-NP	−1.543	ISDN-GER-NP	−1.658
FP-NER-NP	−1.562	DNP -NER-NP	−1.520	ISDN-NER-NP	−1.566
FP-GER-C14-NP	−2.111	DNP-GER-C14-NP	−2.119	ISDN-GER-C14-NP	−1.879
FP-NER-C14-NP	−2.061	DNP-NER-C14-NP	−1.848	ISDN-NER-C14-NP	−1.850

The unit of Hydrogen bond energy is kcal/mol.

more experiments to prove, and our research group has not given much explanation.

3.4. *Identification of drug-SC interaction*

3.4.1. *Molecular docking*

Ceramide is a lipophilic part of SC and is thought to be the most effective element for maintaining skin barrier function due to the formation of a tight hydrogen bond network on the head [28]. CER NP (NP), equivalent to human ceramide 3, was chosen as the skin lipid bilayer model [29, 30]. In the current study, NP was first selected as a receptor, and then the drug or enhancer was participated to the module. Typical snapshots of the minimum energy complexes are displayed in Fig. 6, and the corresponding distances between the two atoms are marked. The total energy of the mixtures is expressed in Table 5. A hydrogen bond (H-bond) was formed when the distance between the hydrogen bond donor and acceptor was less than 3.5 Å [31], as shown Fig. 6. In all systems, the penetration enhancer and the model drugs all formed H-bonds with NP. In addition, the values of blending energy were usually negative, representing that the interplay of NP assemblies with drugs or enhancers was feasible, and a higher absolute value of blending energy indicated that the blending system was more stable. Among all these enhancers, the energy of drug-enhancer-NPs was higher than the energy of drug-NPs, suggesting that selected enhancers interacted more strongly with ceramide. Therefore, it could be considered that the enhancers had the capability to decrease the interaction between the drug and SC and to disrupt the tight network of ceramide, thus entering the enhancers into the lipid bilayers of SC [32]. Moreover, GER-C14 provided the highest docking energy, which might indicate that it had the best optimal attachment to the polar groups of ceramide. GER-C14 could competitively interact with the polar groups of lipids, which provided a possible exposition for its optimal enhancing ability.

3.4.2. *Molecular dynamics simulation*

Through molecular dynamics simulation (MD), the details of the dynamic molecular interaction between enhancer and SC in the lipid bilayer were discussed, as shown in Fig. 7. Fig. 7A-7C&7E were the interaction between GER, NER, GER-C14, NER-C14 and 128DPPC and showed that the hydrogen bonds were appeared in the hydrophilic area of SC. In addition, Fig. 7D&7F also showed another form of interaction between GER-C14, NER-C14 and 128DPPC, which were inserted into the middle of the lipid bilayer to form an independent phase, which

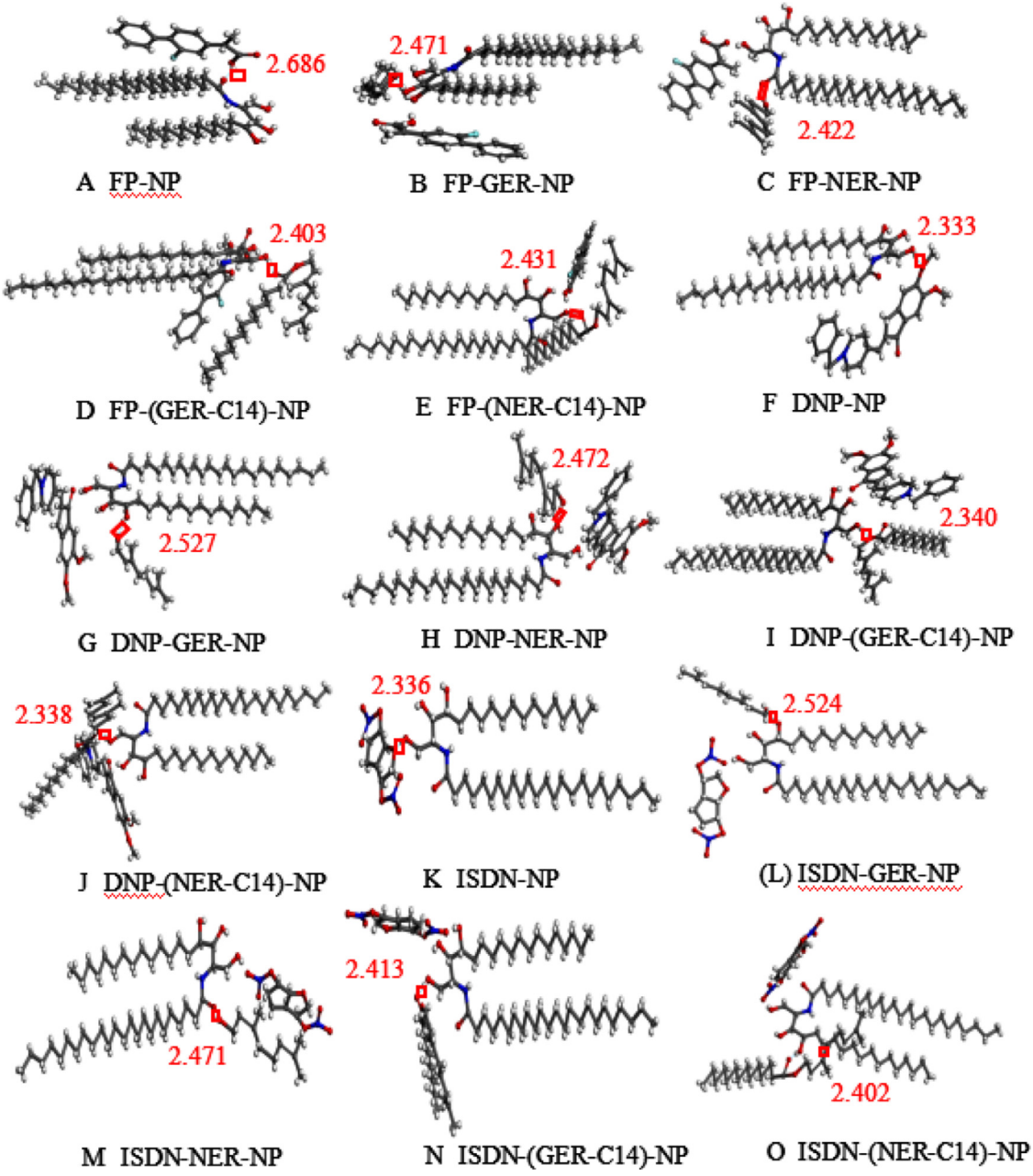

Fig. 6 – The molecular models of drugs, enhancers and NP. Gray: carbon; red: oxygen; blue: nitrogen; white: hydrogen; cyan: fluorine. H-bonds were presented in light blue dotted lines.

might be caused lipids extraction. By comparing with MS, both experimental methods showed that the enhancer could form hydrogen bonds with the head region of the lipid bilayer. In addition, in MD, the dynamic change of the enhancer in the keratin was obtained, that was, it could be inserted into the lipid double layer. This explained on the other hand that the enhancement activity of GER-C14, NER-C14 were stronger than that of GER, NER.

3.5. *ATR-FTIR*

ATR-FTIR was an effective method to find out enhancer-skin interactions by observing the changes in the involved functional groups of skin [33]. The spectra are shown in Fig. 8. The lipid showed its characteristic absorption peak of the symmetrical vibrational absorption peak and asymmetric vibrational absorption peak of CH_2 at 2848.69 cm^{-1} ($\upsilon_s CH_2$) and 2918.12 cm^{-1} ($\upsilon_{as} CH_2$). The characteristic absorption peak of keratin is the amide I band (1639.39 cm^{-1}), representing the secondary structure of the protein [29]. In addition, the water absorbance band was found in the 3278.79 cm^{-1} region.

Compared to the control group, both $\upsilon_s CH_2$ and $\upsilon_{as} CH_2$ in the other groups except for NER-C14 moved to higher wavenumbers, and the displacement of $\upsilon_s CH_2$ in the GER-C14 groups was greater than the displacement of others. Research has shown that the displacement of the CH_2 stretching

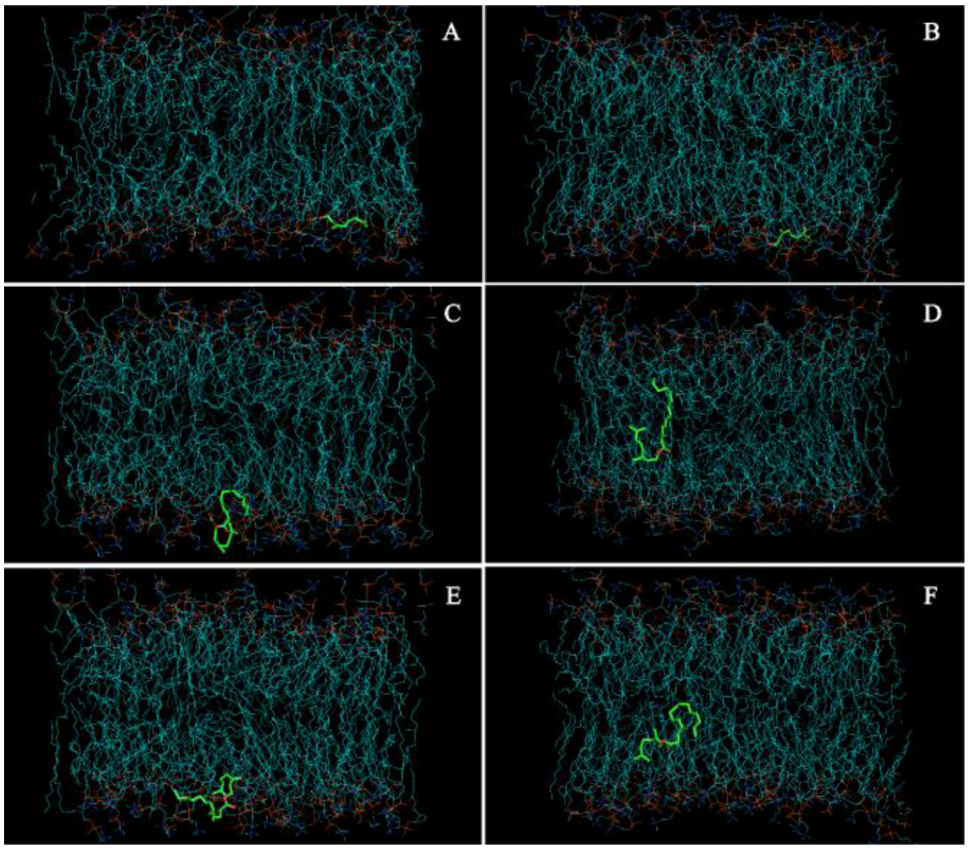

Fig. 7 – The molecular models of enhancers and DPPC. (A) GER; (B) NER; (C, D) GER-C14; (E, F) NER-C14.

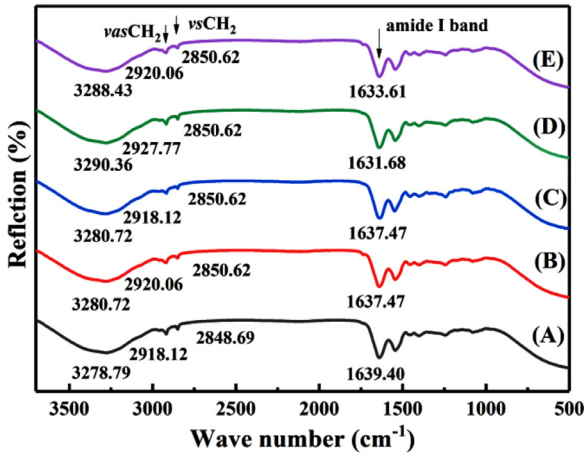

Fig. 8 – ATR-FTIR spectra with or without penetration enhancers. (A) control; (B) GER; (C) NER; (D) GER-C14; (E) NER-C14 ($n = 3$).

vibration peak is concerned to the ratio of CH_2 deflection/total reflection conformer, reflecting the level of freedom of the lipid side chain [30], and the height of these two peaks has been found to be proportional to the amount of lipid pressure in SC. The CH_2 vibration absorption peak moved to a high wavenumber, indicating that CH_2 was deflected, destroying the ordered structure of the lipids and causing a disordered arrangement [34]. The higher displacement of $\upsilon_s CH_2$ in the enhancer group indicated stronger interference with lipid side chains and a greater degree of lipid structure disorder, which can better promote the absorption of the drug. The ATR-FTIR spectrum of SC with enhancers showed a decreased height of $\upsilon_s CH_2$ and $\upsilon_{as} CH_2$ stretching, indicating that lipids were extracted from SC (Table 6). The maximum lipid extraction was obtained by GER-C14, as the peak height decreased the most. The above observation was consistent with the *in vitro* skin permeation results, which obtained the highest accumulation when GER-C14 was added as an enhancer in the patch.

In addition to the change in the CH_2 vibration absorption peak, the displacement value of the amide I band was also changed. As suggested by the shifts of the amide I band from 1639.39 cm^{-1} in control ethanol-treated SC (which represented the change of protein secondary structure [35] to 1637.47 cm^{-1} (GER and NER), 1633.61 cm^{-1} (NER-C14) and 1631.68 cm^{-1} (GER-C14). The reason might be that the steric hindrance and lipophilicity factor of the enhancers squeezed the conformation of the diagonal protein, causing the arrangement of keratins to be deformed, thus increasing the intermolecular space of keratins [36]. The different magnitudes of the displacement by enhancers might be resolved by the acylation of the parent terpenes with myristic acid, which caused changes in molecular size and lipophilicity. Treatment with enhancers resulted in the shift of amide I to a lower wavenumber, which suggested

Table 6 – Peak height of υsCH_2 and $\upsilon asCH_2$ stretching absorbance with or without enhancers and their percentage decrease ($n = 3$).

Treatment	$\upsilon_s CH_2$		$\upsilon_{as} CH_2$	
	Peak height	Decrease in peak height[a] (%)	Peak height	Decrease in peak height[a] (%)
control	0.137	–	0.206	–
GER	0.116	15.3	0.184	10.6
NER	0.117	14.6	0.187	10.6
GER-C14	0.080	41.6	0.138	33.0
NER-C14	0.083	39.5	0.141	31.5

[a] Percentage decrease in peak height: (peak height in control-peak height with enhancer)/peak height in control × 100%.

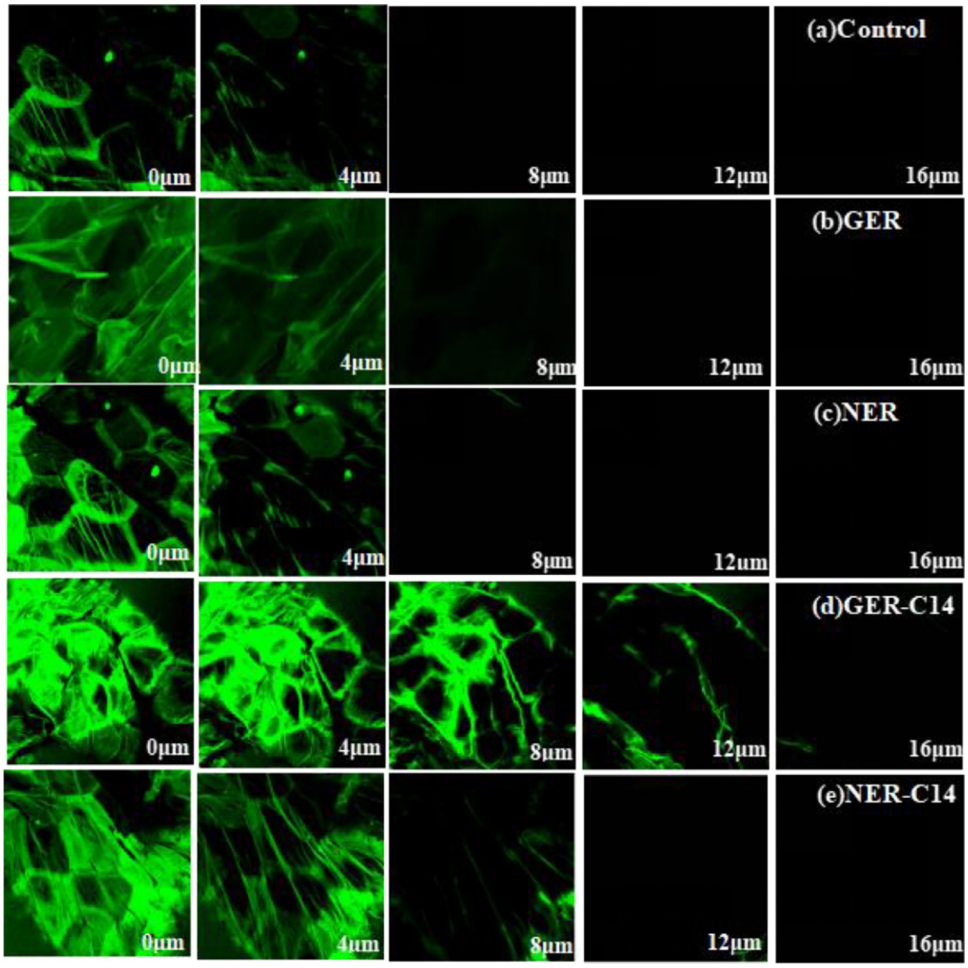

Fig. 9 – CLSM images of rabbit skin at different depths after treatment with different permeation enhancers.

that the hydrogen bond was broken [37]. Furthermore, the vibration absorption peaks of OH in the SC all moved towards higher wavenumbers compared to the control group, which represented the occurrence of hydration that caused the swelling of keratinocytes. Hydration of the epidermis was conducive to the penetration of model drugs, especially hydrophilic drugs. In summary, regardless of the stretching vibration of CH_2, amide I band and -OH group, the GER-C14 group had the largest wave digit shift, which provided a reasonable explanation for its strongest penetration promotion ability and indicated that the structure of (*trans/cis*) configuration isomers had different effects on disturbing SC lipids, promoting protein secondary structure transformation and facilitating cuticle hydration.

3.6. CLSM

The model drug could not be observed directly by CLSM, and fluorescein was selected as the probe to explore the mechanism of permeability promotion of enhancers [38–41]. CLSM was used to display the skin permeation procedure of fluorescein under the influence of enhancers (GER, NER,

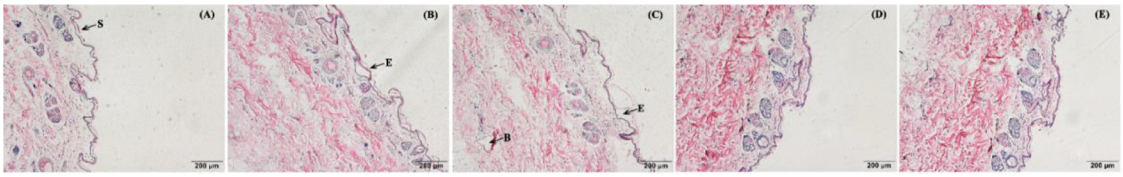

Fig. 10 – Histological pictures of skin treated with various enhancers: (A) control; (B) GER; (C) NER; (D): GER-C14; (E) NER-C14, where S, SC; E, edema; B, bullae formation (H&E 10 ×).

Table 7 – Skin irritation experiments results.

Treatment	Integral mean				Stimulus intensity			
	2h	12h	24h	48h	2h	12h	24h	48h
control	0	0	0	0	–	–	–	–
GER	0	0	0	0	–	–	–	–
NER	0	0	0	0	–	–	–	–
GER-C14	0	0	0	0	–	–	–	–
NER-C14	0	0	0	0	–	–	–	–

"-" represented no skin irritation.

GER-C14, NER-C14). Fig. 9 showed the x-z optical sections of different groups, and the flat hexagonal structure of keratinocytes was observed on the skin surface, which indicated the permeation of fluorescein through the skin by the intercellular lipid pathway. In the control group, the maximum penetration of fluorescein into the skin was 4 μm. When the enhancer was used to pretreat the skin, the penetration depth increased significantly. In the GER, NER, GER-C14, and NER-C14 groups, fluorescein was detected at depths of 8, 8, 16, and 12 μm, respectively, indicating that the selected enhancers had an enhancement effect on the skin and that GER-C14 showed a stronger penetration effect than the others, consistent with the *in vitro* and *in vivo* penetration research. In terms of cell morphology, cells in the GER-C14 and NER-C14 groups showed irregular morphology, suggesting that GER-C14 and NER-C14 contributed to enhancement by disrupting the highly ordered intercellular lipid structure of the SC, thus enhancing drug diffusivity in skin lipids [41].

3.7. *Histological observation*

Histological photomicrographs are depicted in Fig. 10, which shows images of rabbit skin tissue sections with or without enhancer under 10 × magnification. The skin composition and cell morphology without enhancers are shown in Fig. 9A. The SCs arranged in the outermost layer of the epidermis, blood vessels, hair follicles and glands in the dermis and other skin appendages were clearly visible. When the skin was treated with enhancers, the attenuation and abstraction of the lipid bilayer was clearly evident as distinct voids and empty spaces visible in the epidermal area. These results could be related to changes in the conformation of the lipid bilayer [42]. The amphiphilic structure of the enhancer interfered with the arrangement of the lipid bilayer, thereby disrupting the highly organized lipid accumulation in the SC. Furthermore, due to dermal edema in the enhancer group, the dermis layer showed a slight separation of collagen fibers, indicating that the enhancer caused protein modification of the SC [43]. This phenomenon was consistent with the ATR-FTIR results. The changes observed in the tissue sections only indicated the transdermal effect of enhancers, and no apparent signs of skin irritation were observed.

3.8. *Skin irritation test*

According to the skin irritation response scoring standard score, the integral average value of the skin irritation intensity was obtained, and the irritation intensity was evaluated. The results of skin irritation test were shown in Table 7. All experimental groups, after removing the test substance in the test area, the average score is 0, and the statistical scores are all less than 0.50, indicating the skin had no changes of edema, erythema. The selected enhancer was not irritating to the skin and had high safety performance.

4. Conclusions

In conclusion, we could conclude that GER-C14 had the most promoting transdermal absorption ability for different physicochemical drugs with low skin irritation. In addition, its promotion behavior was mediated by promoting drug release, interfering with hydrophilicity by destroying the tight network of ceramide, and loosening lipophilic areas and keratin of SC. In summary, this research provides new ideas for the design of stereoisomer penetration enhancers, and for further research, GER-C14 is expected to be a new permeability enhancer with high efficiency and low toxicity.

Conflict of interest

The authors declare no conflicts of interest.

Acknowledgement

This work was supported by following projects: The Natural Science Foundation of Hebei Province [grant numbers H2019209254], North China University of Science and Technology Foundation for Distinguished Young Scholars [grant numbers JQ201713] and Distinguished Young Scholars of Hebei Province.

Supplementary materials

Supplementary material associated with this article can be found, in the online version, at doi:10.1016/j.ajps.2021.11.003.

REFERENCES

[1] Rai VK, Mishra N, Agrawal AK, Jain S, Yadav NP. Novel drug delivery system: an immense hope for diabetics. Drug Deliv 2016;23(7):2371–90.
[2] Serpe L, Jain A, de Macedo CG, Volpato MC, Groppo FC, Gill HS, et al. Influence of salivary washout on drug delivery to the oral cavity using coated microneedles: an *in vitro* evaluation. Eur J Pharm Sci 2016;93:215–23.
[3] Strasinger C, Raney SG, Tran DC, Ghosh P, Newman B, Bashaw ED, et al. Navigating sticky areas in transdermal product development. J Control Release 2016;233:1–9.
[4] Gratieri T, Alberti I, Lapteva M, Kalia YN. Next generation intra- and transdermal therapeutic systems: using non- and minimally-invasive technologies to increase drug delivery into and across the skin. Eur J Pharm Sci 2013;50(5):609–22.
[5] Karande P, Mitragotri S. Enhancement of transdermal drug delivery via synergistic action of chemicals. Biochim Biophys Acta 2009;1788(11):2362–73.
[6] Vaddi HK, Ho PC, SY Chan. Terpenes in propylene glycol as skin-penetration enhancers: permeation and partition of haloperidol, Fourier transform infrared spectroscopy, and differential scanning calorimetry. J Pharm Sci 2002;91(7):1639–51.
[7] Aqil M, Ahad A, Sultana Y, Ali A. Status of terpenes as skin penetration enhancers. Drug Discov Today 2007;12(23–24):1061–7.
[8] Kanikkannan N, Kandimalla K, Lamba SS, Singh M. Structure-activity relationship of chemical penetration enhancers in transdermal drug delivery. Curr Med Chem 2000;7(6):593–608.
[9] Arellano A, Santoyo S, Martin C, Ygartua P. Enhancing effect of terpenes on the *in vitro* percutaneous absorption of diclofenac sodium. Int J Pharm 1996(1):130.
[10] Godwin DA, Michniak BB. Influence of drug lipophilicity on terpenes as transdermal penetration enhancers. Drug Dev Ind Pharm 1999;25(8):905–15.
[11] Charoo NA, Anwer A, Kohli K, Pillai KK, Rahman Z. Transdermal delivery of flurbiprofen: permeation enhancement, design, pharmacokinetic, and pharmacodynamic studies in albino rats. Pharm Dev Technol 2005;10(3):343–51.
[12] Choi J, Choi MK, Chong S, Chung SJ, Shim CK, Kim DD. Effect of fatty acids on the transdermal delivery of donepezil: *in vitro* and *in vivo* evaluation. Int J Pharm 2012;422(1–2):83–90.
[13] Zhao JH, Fu JH, Wang SM, Su CH, Shan Y, Kong SJ, et al. A novel transdermal patch incorporating isosorbide dinitrate with bisoprolol: *in vitro* and *in vivo* characterization. Int J Pharm 2007;337(1–2):88–101.
[14] Sun L, Cun D, Yuan B, Cui H, Xi H, Mu L, et al. Formulation and *in vitro/in vivo* correlation of a drug-in-adhesive transdermal patch containing azasetron. J Pharm Sci 2012;101(12):4540–8.
[15] Nielsen JB. Natural oils affect the human skin integrity and the percutaneous penetration of benzoic acid dose-dependently. Basic Clin Pharmacol Toxicol 2006;98(6):575–81.
[16] Ibrahim SA, Li SK. Chemical enhancer solubility in human stratum corneum lipids and enhancer mechanism of action on stratum corneum lipid domain. Int J Pharm 2010;383(1–2):89–98.
[17] Vávrová K, Zbytovská J, Hrabálek A. Amphiphilic transdermal permeation enhancers: structure-activity relationships. Curr Med Chem 2005;12(19):2273–91.
[18] Kunta JR, Goskonda VR, Brotherton HO, Khan MA, Reddy IK. Effect of menthol and related terpenes on the percutaneous absorption of propranolol across excised hairless mouse skin. J Pharm Sci 1997;86(12):1369–73.
[19] Warner KS, Li SK, Higuchi WI. Influences of alkyl group chain length and polar head group on chemical skin permeation enhancement. J Pharm Sci 2001;90(8):1143–53.
[20] He N, Li SK, Suhonen TM, Warner KS, Higuchi WI. Mechanistic study of alkyl azacycloheptanones as skin permeation enhancers by permeation and partition experiments with hairless mouse skin. J Pharm Sci 2003;92(2):297–310.
[21] Riviere JE, Papich MG. Potential and problems of developing transdermal patches for veterinary applications. Adv Drug Deliv Rev 2001;50(3):175–203.
[22] Uppoor VR. Regulatory perspectives on *in vitro* (dissolution)/*in vivo* (bioavailability) correlations. J Control Release 2001;72(1–3):127–32.
[23] Yang Y, Manda P, Pavurala N, Khan MA, Krishnaiah YS. Development and validation of *in vitro-in vivo* correlation (IVIVC) for estradiol transdermal drug delivery systems. J Control Release 2015;210:58–66.
[24] Chu T, Wang C, Wang J, Wang H, Geng D, Wu C, et al. Chiral 4-O-acylterpineol as transdermal permeation enhancers: insights of the enhancement mechanisms of a transdermal enantioselective delivery system for flurbiprofen. Drug Deliv 2020;27(1):723–35.
[25] Zhao H, Liu C, Yang D, Wan X, Shang R, Quan P, et al. Molecular mechanism of ion-pair releasing from acrylic pressure sensitive adhesive containing carboxyl group: roles of doubly ionic hydrogen bond in the controlled release process of bisoprolol ion-pair. J Control Release 2018;289:146–57.
[26] Liu C, Guan Y, Tian Q, Shi X, Fang L. Transdermal enhancement strategy of ketoprofen and teriflunomide: the effect of enhanced drug-drug intermolecular interaction by permeation enhancer on drug release of compound transdermal patch. Int J Pharm 2019;572:118800.
[27] Song W, Quan P, Li S, Liu C, Lv S, Zhao Y, et al. Probing the role of chemical enhancers in facilitating drug release from patches: mechanistic insights based on FT-IR spectroscopy, molecular modeling and thermal analysis. J Control Release 2016;227:13–22.
[28] Jain AK, Thomas NS, Panchagnula R. Transdermal drug delivery of imipramine hydrochloride. I. Effect of terpenes. J Control Release 2002;79(1–3):93–101.
[29] Imura T, Sakai H, Yamauchi H, Kaise C, Kozawa K, Yokoyama S, et al. Preparation of liposomes containing Ceramide 3 and their membrane characteristics. Colloids Surf B 2001;20(1):1–8.
[30] Rerek ME, Van Wyck D, Mendelsohn R, Moore DJ. FTIR spectroscopic studies of lipid dynamics in phytosphingosine ceramide models of the stratum corneum lipid matrix. Chem Phys Lipids 2005;134(1):51–8.

[31] Liu C, Quan P, Li S, Zhao Y, Fang L. A systemic evaluation of drug in acrylic pressure sensitive adhesive patch *in vitro* and *in vivo*: the roles of intermolecular interaction and adhesive mobility variation in drug controlled release. J Control Release 2017;252:83–94.
[32] Wu PC, Chang JS, Huang YB, Chai CY, Tsai YH. Evaluation of percutaneous absorption and skin irritation of ketoprofen through rat skin: *in vitro* and *in vivo* study. Int J Pharm 2001;222(2):225–35.
[33] Boncheva M, Damien F, Normand V. Molecular organization of the lipid matrix in intact Stratum corneum using ATR-FTIR spectroscopy. Biochim Biophys Acta 2008;1778(5):1344–55.
[34] Mendelsohn R, Flach CR, Moore DJ. Determination of molecular conformation and permeation in skin via IR spectroscopy, microscopy, and imaging. Biochim Biophys Acta 2006;1758(7):923–33.
[35] Tatulian SA. FTIR analysis of proteins and protein-membrane interactions. Methods Mol Biol 2019;2003:281–325.
[36] Ibrahim SA, Li SK. Effects of chemical enhancers on human epidermal membrane: structure-enhancement relationship based on maximum enhancement (E(max)). J Pharm Sci 2009;98(3):926–44.
[37] Ahad A, Aqil M, Ali A. The application of anethole, menthone, and eugenol in transdermal penetration of valsartan: enhancement and mechanistic investigation. Pharm Biol 2016;54(6):1042–51.
[38] Li Y, Wang C, Wang J, Chu T, Zhao L, Zhao L. Permeation-enhancing effects and mechanisms of O-acylterpineol on isosorbide dinitrate: mechanistic insights based on ATR-FTIR spectroscopy, molecular modeling, and CLSM images. Drug Deliv 2019;26(1):107–19.
[39] Chen Y, Cun D, Quan P, Liu X, Guo W, Peng L, et al. Saturated long-chain esters of isopulegol as novel permeation enhancers for transdermal drug delivery. Pharm Res 2014;31(8):1907–18.
[40] Li N, Quan P, Wan X, Liu C, Liu X, Fang L. Mechanistic insights of the enhancement effect of sorbitan monooleate on olanzapine transdermal patch both in release and percutaneous absorption processes. Eur J Pharm Sci 2017;107:138–47.
[41] Zhao H, Liu C, Quan P, Wan X, Shen M, Fang L. Mechanism study on ion-pair complexes controlling skin permeability: effect of ion-pair dissociation in the viable epidermis on transdermal permeation of bisoprolol. Int J Pharm 2017;532(1):29–36.
[42] Prasad R, Koul V, Anand S, Khar RK. Effect of DC/mDC iontophoresis and terpenes on transdermal permeation of methotrexate: *in vitro* study. Int J Pharm 2007;333(1–2):70–8.
[43] Amin S, Kohli K, Khar RK, Mir SR, Pillai KK. Mechanism of *in vitro* percutaneous absorption enhancement of carvedilol by penetration enhancers. Pharm Dev Technol 2008;13(6):533–9.